Photostereochemistry and Photoaquation Reactions of [Cr(tn)3]3+: Theoretical Studies Show the Importance of Reduced Coordination Conical Intersection Geometries

Zurek, Justyna Marlena; Paterson, Martin J

Published in:
Journal of Physical Chemistry A

DOI:
10.1021/jp302300q

Publication date:
2012

Document Version
Publisher's PDF, also known as Version of record

THE JOURNAL OF PHYSICAL CHEMISTRY A

Article

pubs.acs.org/JPCA

Photostereochemistry and Photoaquation Reactions of $[Cr(tn)_3]^{3+}$: Theoretical Studies Show the Importance of Reduced Coordination Conical Intersection Geometries

Justyna M. Żurek and Martin J. Paterson*

Institute of Chemical Sciences, School of Engineering and Physical Sciences, Heriot-Watt University, Edinburgh, Scotland EH14 4AS

Supporting Information

ABSTRACT: We have performed TD-DFT and CASSCF calculations to understand the spectroscopy and reactive photochemistry of the $[Cr(tn)_3]^{3+}$ complex. Our results show that, after population of a quartet ligand field excited state, the system relaxes by dissociation of a Cr−N bond to reach a quasi-trigonal bipyramid five-coordinate species that is a conical intersection connecting the excited and ground quartet manifolds. Nonadiabatic relaxation through these leads to square pyramidal structures that can coordinate water and account for the observed monoaquated photoproducts. Such features are also present on the potential energy surfaces of these photoproducts and account for the range of experimentally observed photostereoisomers of the photoaquation reactions.

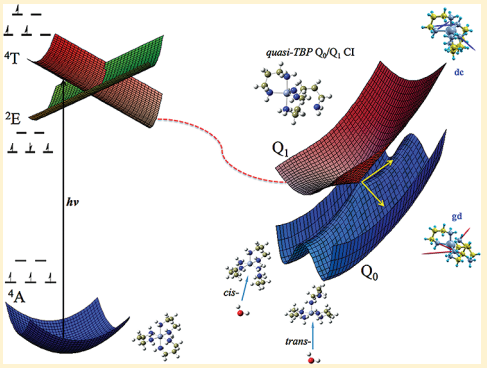

INTRODUCTION

Chromium(III)−amine complexes have been of general interest for many years.[1,2] Their photochemistry in particular, as part of the photochemistry of Cr(III) complexes in general, has been the source of some debate, and many aspects of it are currently not understood and are the cause of some controversy.[3−5] Initially, it was quite cryptic which excited states are responsible for the complex photochemistry observed in Cr(III) complexes, and it proved a challenge for experimentalists to accurately probe the photochemical pathways and relaxation mechanisms in these systems. It is now widely believed that the photochemistry of Cr(III)−amine systems occurs from population of an excited ligand-field quartet state with possible participation from doublet states, after intersystem crossing.[5,6] However, computational studies are required to describe the reactivity and nature of these states and the mechanism(s) of the subsequent photoreactions. A wide variety of photochemical behavior is observed for a range of Cr(III) complexes,[1] although many common features have been observed. We have recently performed calculations on the Cr(III) oxalate complex $[Cr(C_2O_4)_3]^{3-}$,[7] which is known for having similar spectral properties to ruby and for being a good system for energy migration studies due to the lack of exchange interactions when incorporated into stoichiometric compounds. Relaxation pathways through doublet and quartet manifolds and the electronic spectroscopy of this system were described using time-dependent density functional theory (TD-DFT) and the complete active space self consistent field method (CASSCF). These methods when correctly applied in conjunction with each other can give a good insight into the occurring photochemistry of such systems. In this paper, we use a similar methodology to understand and describe the spectroscopy and mechanisms of the photoaquation reactions of the $[Cr(tn)_3]^{3+}$ complex, where tn is 1,3-diaminopropane, and those of its stepwise photoproducts.

The tn ligand belongs to the group of bidentate ligands, which can bond to and form a ring with a metal center through two atoms, in this case the two nitrogen atoms, via lone pairs. Tn ligands can adopt different structures when coordinated to the metal. In the $[Cr(tn)_3]^{3+}$ complex, two tn ligands exhibit a chair conformation while the other one exhibits a twist boat conformation as shown in Figure 1.[8] Also presented is a schematic of the geometric structure of the complex. As discussed below, there is also another local minimum corresponding to two twist boat and one chair conformations. At both of these minima, the metal center is essentially octahedrally coordinated, although the full complex has no symmetry in either (C_1 point group).

The aquation reactions of Cr(III)−amine systems, which involve the incorporation of water molecules to the metal center, are found to be photoinduced and can occur through different pathways on the quartet and doublet spin manifolds providing for different photoproducts. The incorporation of a water molecule can cause the displacement of other ligands present. A common feature of the photoaquation reaction in Cr(III)−amine complexes is that this process is very efficient, and the reaction can be partially quenchable via the involvement of photoactive doublet states or with different

Received: March 9, 2012
Revised: May 1, 2012
Published: May 10, 2012

dx.doi.org/10.1021/jp302300q | J. Phys. Chem. A 2012, 116, 5375−5382

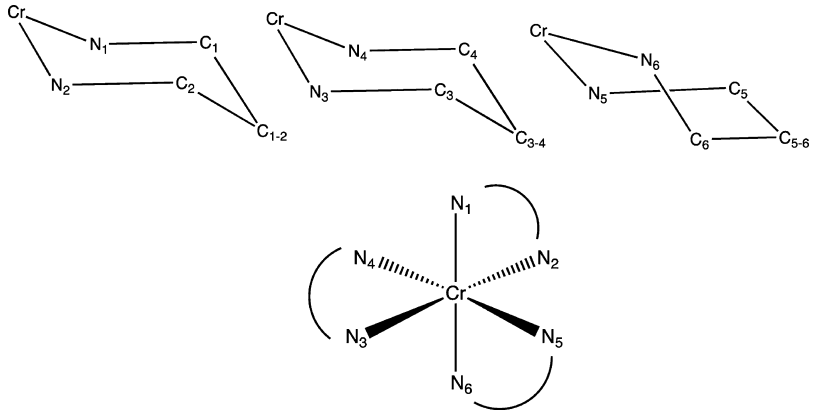

Figure 1. Pictorial representation of structural parameters of the $[Cr(tn)_3]^{3+}$ complex: (a) two tn ligands in chair conformation, (b) tn ligand in twist boat conformation, and (c) full complex (the N−N bridge here is $CH_2CH_2CH_2$).

reaction quenchers.[3,9,10] Quenchers are molecules that absorb the emission energy of other nearby molecules, and it has been found that the type of quencher used in the reaction can influence the final photostereochemistry of the system.

There have been many studies on groups of complexes containing different amine ligand analogues such as NH_3, cyclam (cyclam = 1,4,8,11-tetraazacyclotetradecane), en (en = 1,2-diaminoethane), or tn (tn = 1,3-diaminopropane).[2,11,12] The ring size and thus the steric effects of the ligands can influence the quantum yields of the reactions.[9] Studies show that these systems possess similar spectral properties. However, their photochemistry and ligand substitution reactions may be quite different depending on the type of ligands present.

Early experimental studies on the $[Cr(tn)_3]^{3+}$ complex suggested two possible main products of the photoaquation reaction, one being the $[Cr(tn)_2(tnH)(H_2O)]^{4+}$ complex and the other the $[Cr(tn)_2(H_2O)_2]^{3+}$ complex, both in their *cis* and *trans* forms.[13] Here, tnH denotes the tn ligand bound through one nitrogen only with the other amino group protonated. Initially, it was thought that the production of the $[Cr(tn)(tnH)_2(H_2O)_2]^{5+}$ complex could occur via secondary photolysis or thermal aquation of the first photoproduct, the $[Cr(tn)_2(tnH)(H_2O)]^{4+}$ complex. However, this was later ruled out on account of low conversion. The presence of the *trans* isomer of the $[Cr(tn)_2(H_2O)_2]^{3+}$ complex was dismissed on a spectroscopic basis.[13] The formation of diaquo products through thermal aquation of the first photoproduct was also excluded due to the very slow rate, and it was then suggested that the formation of the diaquo complex $[Cr(tn)_2(H_2O)_2]^{3+}$ occurs directly from the photoaquation of $[Cr(tn)_3]^{3+}$. Such experimental hypotheses require detailed computational modeling to fully reconcile.

Experimental studies further show that the formation of the monoaquo $[Cr(tn)_2(tnH)(H_2O)]^{4+}$ complex occurs with a low quantum yield of 0.15, which the authors explained as a result of the quite high stability of the tn ligand, which turned out to be much more stable than other amine analogues. This is due to its conformation of a six-membered chair ring, as in cyclohexane, while bonding to the metal, that also made it a much poorer leaving group compared to other amine analogues.[14,15] Gowin and Wasgestian suggested that fast rechelation of this system can be the reason of the low quantum yields observed for photoaquation.[13] This rechelation reaction can compete with protonation of the detached ligand, which after being protonated blocks a coordination site. However, the quantum yield was found to be independent of the acid concentration; thus, the rechelation reaction is much faster than protonation. The quantum yield of the $[Cr(tn)_2(H_2O)_2]^{3+}$ product was equal to 0.04. The hydroxide ion was present in the mixture as a reaction quencher.[13] The photoaquation reaction of the $[Cr(tn)_3]^{3+}$ complex was then reinvestigated, together with extensive studies on reaction quenching by $Na[Cr(tn)(CN_4)]$ in comparison with the OH^- quencher. This complex turned out to be a very efficient quencher of the reaction, which does not absorb over the wavelength range 450−735 nm and can be used over a large pH range of 2−10, unlike OH^-. The product mixture contained the initial complex $[Cr(tn)_3]^{3+}$, *cis* and *trans* isomers of $[Cr(tn)_2(tnH)(H_2O)]^{4+}$, the $[Cr(tn)(tnH)_2(H_2O)_2]^{5+}$ complex that was not observed before, and another unidentified secondary photoproduct. The use of a quencher and the type of quencher seemed to have an influence on the *cis* and *trans* isomer ratios of the photoproducts. The quantum yield was the same for doublet- and quartet-state irradiation. The effect of the increase in the percentage of *cis* isomer in the red edge of the spectrum of the quartet absorption band, which was observed in previous studies, was not reproduced. The authors stated that previous results may have been due to possible errors in the peak area measurements or more likely to parallel thermal reactions during photolysis.[15] The aquation reaction of the $[Cr(tn)_3]^{3+}$ complex through the transition-state pathway on a ground-state PES was not observed experimentally and was excluded due to steric effects blocking the incoming ligand.[2]

Thus, given these differing experimental results and in general the lack of mechanistic understanding of this important class of photochemical reactions, computational modeling of the possible photochemical pathways from initial excitation to product formation are timely. This paper focuses on such a computational study of both the initial electronic spectroscopy and characterization of the electronic states involved as well as excited-state pathways involving nonadiabatic channels leading to the radiationless generation of coordinatively unsaturated photoproducts that subsequently coordinate water to form the observed aquated photostereoisomers.

■ COMPUTATIONAL DETAILS

DFT structure optimizations of the $[Cr(tn)_3]^{3+}$ complex and its possible photoproducts such as *cis*- and *trans*-$[Cr(tn)_2(H_2O)_2]^{3+}$, and *cis*- and *trans*-$[Cr(tn)_2(tnH)(H_2O)]^{4+}$ have been performed using the B3LYP functional with two

dx.doi.org/10.1021/jp302300q | J. Phys. Chem. A 2012, 116, 5375−5382

Table 1. Spectral Bands of the $[Cr(tn)_3]^{3+}$ Complex and Main Photoaquation Products Obtained from TD-DFT

complex	wavelength (nm)	characterization	experiment[c] (nm)	characterization
$[Cr(tn)_3]^{3+}$	420[d]	LF	457	LF
	345[d]	LF	351	LF
	240	LMCT		
cis-$[Cr(tn)_2(H_2O)_2]^{3+}$	450[e]	LF	–	–
	360[e]	LF		
	335[e]	LF		
	265	LMCT		
trans-$[Cr(tn)_2(H_2O)_2]^{3+}$	545[d]	LF	–	–
	491[d]	LF		
	432[d]	LF		
	386[d]	LF		
	320	LMCT		
	270	LMCT		
	205	LMCT		
cis-$[Cr(tn)_2(tnH)(H_2O)]^{4+}$	480[e]	LF	–	–
	435[e]	LF		
	345[e]	LF		
	270	LMCT		
	205	very mixed		
trans-$[Cr(tn)_2(tnH)(H_2O)]^{4+}$	512[d]	LF	–	–
	487[d]	LF		
	421[d]	LF		
	397[d]	LF		
	310	LMCT[a]		
	265	LMCT[b]		
	240	LMCT[b]		
	205	LMCT[b]		

[a]Small mixing with LF states. [b]Mixing with IL states. [c]UV−vis.[13] [d]Oscillator strength equal 0. [e]Weak intensity (oscillator strength between 0.0001 and 0.0007).

basis set variations: first an SDD effective core potential (1s2s2p 10 electron core) basis set for Cr and the 6-31G(p,d) for the C, O, N, and H atoms; second an all-electron cc-pVTZ basis set for all the atoms, with the metal set from Peterson et al.[16] The ground-state geometry results did not differ significantly between different basis sets used for the B3LYP calculations.

The structural parameters of only the $[Cr(tn)_3]^{3+}$ complex obtained in these calculations together with CASSCF optimization results and their comparison with experimental studies of the crystal structure are presented in Table S1 of the Supporting Information. The schematic representation of structural parameters present in this Table is shown in Figure 1.

TD-B3LYP was used to investigate the vertically excited electronic states. Again, the spectrum was relatively insensitive to the basis set, and the results using SDD ECP for Cr and using 6-31G(p,d) for C, O, N, and H atoms are given above (Table 1). To determine the character of the states the dominant component of the transition was chosen. Some of the states involved a large degree of state mixing, and so they were harder to resolve. For those states natural transition orbitals (NTOs) were generated. This creates a compact orbital representation of the electronic transition density matrix and often aids the assignment of electronic spectra from response theory.

Photochemical pathways for $[Cr(tn)_3]^{3+}$ leading to various photoproducts were investigated using the CASSCF method. Such multiconfigurational wave functions are essential to treat open-shell ground and excited states, especially for a qualitative treatment of a range of effects induced by vibronic coupling such as conical intersection or intersystem crossing seams. An active space based on natural orbital occupations was chosen using the CAS-UNO method.[17,18] Initial guess natural orbitals were generated from a UHF wave function. Natural orbitals are the orbitals that diagonalize the one-electron density matrix and whose eigenvalues are occupation numbers that give a measure of the importance of that orbital in a multiconfigurational wave function. The use of natural orbitals has proved successful in cases where the initial choice of orbitals for the CASSCF wave function has been unclear or problematic due to system size. This method of generating CASSCF wave functions has been demonstrated on organic molecules,[17,18] and recently, we used this method successfully in a study of the *meridial* to *facial* photoisomerisation of a large platinum(IV) amido Pincer-type complex.[19] For a chromium(III) complex, the minimal size of active space to cover all the metal d orbitals is a (3,5). However, as has been shown previously, larger active spaces are generally required to account for dative metal−ligand bonding.[19−26] Such expanded active spaces account for additional dynamic correlation and give qualitative wave functions that are capable of producing good geometries and reasonable relative energetics such as barrier heights (e.g., conical intersections and pseudorotation barrier heights in transition metal carbonyls[21,23−25]). The advantage of such wave functions for the ground and LF states is that analytical gradients, Hessians, and nonadiabatic couplings are then available and facilitate the study of the mechanistic reactive photochemistry. For accurate spectroscopy and comparison of the relative energetics between for example LMCT and LF states, multireference perturbation corrections, such as CASPT2, are essential. Here, the expanded

active space was chosen from the UNO occupation numbers, and the best balance was found to be an active space containing 9 electrons and 10 orbitals, generating 25 200 quartet Slater determinant configurations. This active space was further expanded, and a couple of selected geometries discussed below were reoptimised. Only a very small effect on geometrical parameters was observed. The one-electron basis set used for the CASSCF calculations was the same as for the TD-DFT calculations as discussed above. Conical intersection searches were performed in order to determine the relaxation pathways in the quartet and doublet manifolds in these systems. For the conical intersection optimization with CASSCF, the orbital rotation terms were neglected in the solution of the coupled perturbed multiconfiguration self-consistent field (CP-MCSCF) equations. An intersystem crossing search between quartet and doublet states was performed using the same optimization algorithm as for the conical intersection search using the CASSCF method. For these, the many electron basis consisted of M_S = $^1/_2$ Slater determinants. Such a many electron basis is capable of describing all spin states that share a common M_S eigenvalue. At points of intersystem crossing, the derivative coupling vector is equal to zero because of the different spin symmetries of these states, and only the gradient difference vector is nonzero. An intersystem crossing seam search using CASSCF was applied in our recent paper on the photoracemization of chromium(III) oxalate ions in which the intersystem crossing seam between ^{4}T and ^{2}E states was located.[7] All computations discussed above were performed with the Gaussian 09 program.[27]

RESULTS AND DISCUSSION

Table 1 presents the absorption bands and their character for the $[Cr(tn)_3]^{3+}$ complex and the main photoproducts generated (the nature of these is discussed further below). States at wavelengths longer than 330 nm are of ligand field character and involve mainly the excitations between the t_{2g} and e_g sets of orbitals. For octahedral systems, having inversion symmetry, these transitions are electronically (Laporte) forbidden. In cases where the system lowers its symmetry, for example, due to vibronic coupling present (e.g., Jahn–Teller distortions), the Laporte rule is no longer strictly valid. The studied complex has only quasi-O_h symmetry at the metal center. This thus explains the presence of weak LF transitions (oscillator strength in the range 0.0001–0.0007) here. The higher-energy bands of the spectrum involved mainly excitations of ligand to metal charge transfer character.

The ground-state minimum of $[Cr(tn)_3]^{3+}$ and its photoaquation products all have quartet spin states. To determine possible relaxation pathways in the quartet manifold of the reaction, a search for surface crossings of the $[Cr(tn)_3]^{3+}$ complex has been performed using CASSCF as detailed above. A conical intersection seam has been located between the quartet ground state of $(d_{xz})^1(d_{yz})^1(d_{xy})^1$ configuration, and the quartet excited state of $(d_{xz})^1(d_{yz})^1(d_{x^2-y^2})^1$ configuration, which involves a rupture of a single Cr–N bond that comes from a tn ligand of twist boat conformation and the rearrangement of the ligands to form a trigonal bipyramidal geometry (TBP) at the metal center. Figure 2 presents the d orbital splittings on going from a six-coordinate octahedral to five-coordinate TBP geometry.

The d_{xy} and $d_{x^2-y^2}$ orbitals for a TBP geometry at the metal center become degenerate, and they are equally populated. Looking at the CASSCF wave function presented in Table 2 at the point of conical intersection, where the system has a quasi-TBP geometry, this is indeed the case. There is almost 50% of the electron density in each of these two orbitals. The derivative coupling (dc) and gradient difference (gd) vectors are plotted in Figure 3. These define the geometrical displacements that lift the degeneracy at first order in nuclear motion away from the TBP conical intersection. It can be seen that these essentially involve a rearrangement of the bonded ligands to adopt a more square pyramidal coordination around the metal.

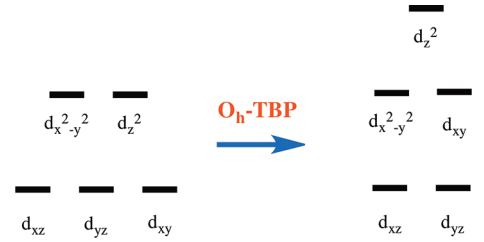

Figure 2. Splitting of metal 3d orbitals from an octahedral geometry (O_h) to trigonal bipyramidal (TBP).

Table 2. Metal d Orbital Occupations of $[Cr(tn)_3]^{3+}$ and $[Cr(tn)_2]^{2+}$ Species on the Ground-State Potential Energy Surface (PES) and at the Minimum Energy Q_0/Q_1 Conical Intersection[a]

$[Cr(tn)_3]^{3+}$				
d_{xz}	d_{yz}	d_{xy}	d_{z^2}	$d_{x^2-y^2}$
Ground-State PES				
0.9999	0.9999	0.9999	0.0180	0.0185
Conical Intersection				
1.0001	0.9999	0.5039	0.0212	0.5001
$[Cr(tn)_2]^{2+}$				
d_{xz}	d_{yz}	d_{xy}	d_{z^2}	$d_{x^2-y^2}$
Ground-State PES				
1.0001	0.99997	0.9974	0.04995	0.0376
Conical Intersection				
0.9999	0. 9998	0. 5025	0.0371	0.5049

[a]CASSCF with SDD ECP basis for Cr and 6-31g(p,d) for C, O, N, and H atoms.

Geometry optimizations starting on the ground state at a geometry displaced away from the conical intersection in the direction of the gradient difference vector were performed using DFT (B3LYP functional). Two stable minima with square pyramidal geometry at the metal center were found, both having a coordination hole at the axial position at the metal center and one tn ligand "hanging loose" as shown in Figure 3. Water can then coordinate to the metal on the ground-state PES. This leads to formation of both *cis* and *trans* isomers of the $[Cr(tn)_2(tnH)(H_2O)]^{4+}$ complex. Indeed, its presence has been seen in the experimental studies as one of the products of the photoinduced aquation reaction of $[Cr(tn)_3]^{3+}$.[13,15] The Q_0/Q_1 conical intersection is on a ridge connecting the *cis* and *trans* isomers, and therefore, decay through this will subsequently involve downhill passage to either of the minima in the moat surrounding the intersection.

The presence of both stereoisomers of the $[Cr(tn)_2(tnH)(H_2O)]^{4+}$ system can be explained in a similar way to the photostereochemistry of the five-coordinate chromium fragments described by Vanquickenborne in the case of other Cr(III)–amine systems.[2] Figure 4 presents the schematic picture of the possible isomerization from trigonal bypiramidal

dx.doi.org/10.1021/jp302300q | J. Phys. Chem. A 2012, 116, 5375–5382

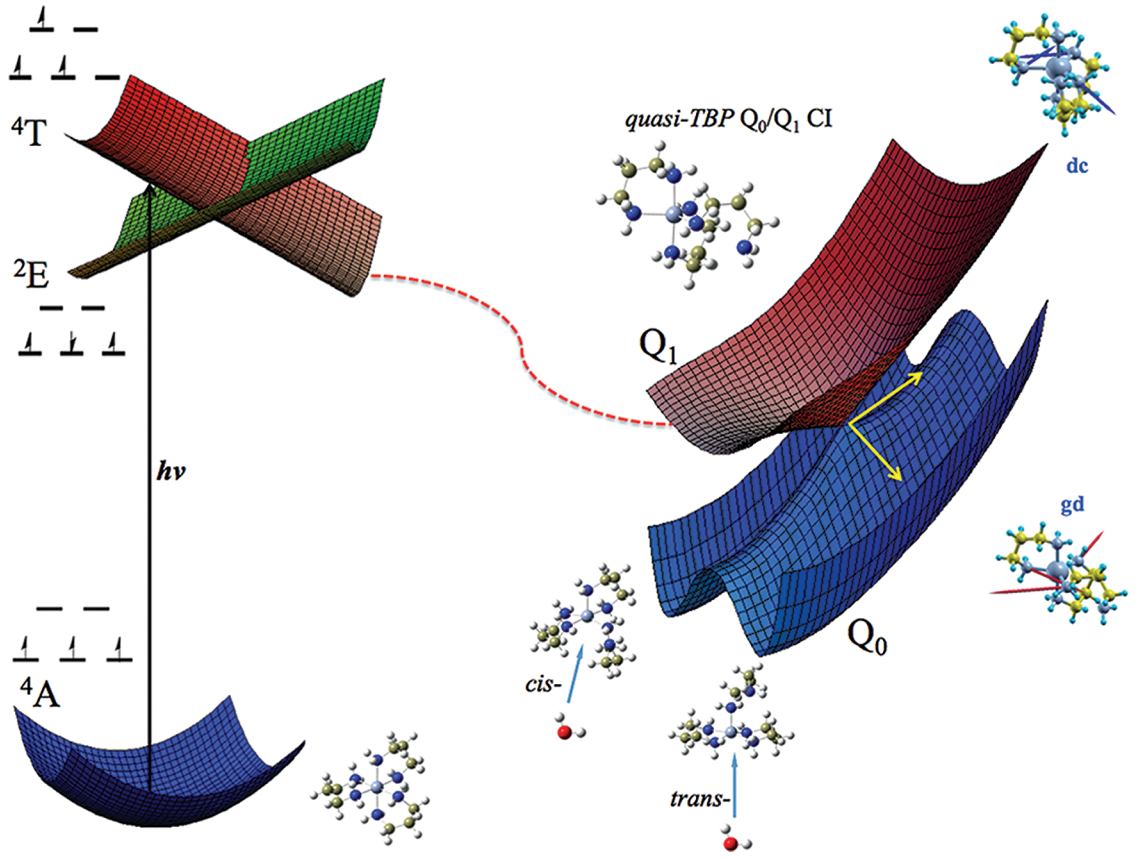

Figure 3. Structures of $[Cr(tn)_3]^{3+}$ complex and schematic representation of possible photoaquation mechanism of this system through a Q_0/Q_1 conical intersection at coordinatively unsaturated quasi-trigonal bipyramid geometry (gd, gradient difference vector; dc, derivative coupling vector).

(TBP) to square pyramidal (SPyr) coordination of the ligands around the metal center. Structure 1 in Figure 4 represents the structure of $[Cr(tn)_3]^{3+}$ at the point of conical intersection with a TBP geometry at the metal center. The equatorial plane contains two nitrogen atoms coming from tn ligands of chair conformation still fully coordinated to the metal and a nitrogen atom at one end of the dissociated tn ligand.

As described in ref 2, the TBP structure is a Jahn–Teller (JT) active geometry that could be accessed by rearrangement of the ligands in the equatorial plane. The equatorial bending modes that are present at the conical intersection point of $[Cr(tn)_3]^{3+}$ could cause the isomerization to SPyr coordination at the metal center. These modes are indeed the calculated dc and gd vectors shown in Figure 3. Structure 2 is formed by the equatorial bending of the N_4CrN_2 angle. Structures 3 and 4 are equivalent and formed due to the equatorial bending vibration of the N_5CrN_2 or N_4CrN_5 angles. The ground-state structures in the presence of water can trap the water molecules, structure 2 in the *trans* position to the one-end dissociated tn ligand and structures 3 and 4 in the *cis* position to a one-end dissociated tn ligand. This would explain the presence of both *cis* and *trans* isomers of the $[Cr(tn)_2(tnH)(H_2O)]^{4+}$ complex.

Summing up, the formation of the $[Cr(tn)_2(tnH)(H_2O)]^{4+}$ photoproduct occurs by the excited-state pathway shown in Figure 3. The $[Cr(tn)_3]^{3+}$ complex, after excitation to the quartet excited state, has access to a very efficient conical intersection connecting to the ground-state PES. The molecule at the point of conical intersection has TBP coordination at the Cr atom, which is similar to the TBP Jahn–Teller active structure common for other Cr (III) complexes, leading to formation of the SPyr isomers on the ground-state PES (Figure 4). A water molecule coordinates to the Cr atom on the ground-state PES leading to the formation of *cis* and *trans* monoaquo isomers $[Cr(tn)_2(tnH)(H_2O)]^{4+}$.

According to the experiment, the photoactive doublet state can participate in the photochemistry of this system and quench the photoreaction. An intersystem crossing seam between the first quartet excited state and a lower lying doublet state (electronic configuration shown in Figure 3) was located, which gives an alternative pathway for relaxation of this system. The presence of this alternative pathway through the doublet excited states may possibly account for the quenching of the aquation reactions.

Similar studies as for the $[Cr(tn)_3]^{3+}$ complex were performed on the main photoproducts of the photoaquation reaction of the $[Cr(tn)_3]^{3+}$system such as the following: *cis*- and *trans*-$[Cr(tn)_2(tnH)(H_2O)]^{4+}$ and *cis*-$[Cr(tn)_2(H_2O)_2]^{3+}$ to look into the stepwise photoproducts that may be formed in any successive reaction. The results of these studies are presented below. The possible relaxation pathways on the quartet manifold of the *cis*-$[Cr(tn)_2tnH(H_2O)]^{4+}$ complex were examined with CASSCF using the same type of active space as discussed above. A conical intersection was located connecting the quartet ground state with the first quartet excited state. The characteristic geometrical feature of the conical intersection point for this system is as for the previous complex; a rupture of a Cr–N bond of one of the tn ligands, this time of chair conformation. The structure at the conical intersection point ($[Cr(tn)(tnH)_2(OH)]^{3+}$) is shown in Figure 5b). The chromium center again adopts a TBP structure that can distort

dx.doi.org/10.1021/jp302300q | J. Phys. Chem. A 2012, 116, 5375–5382

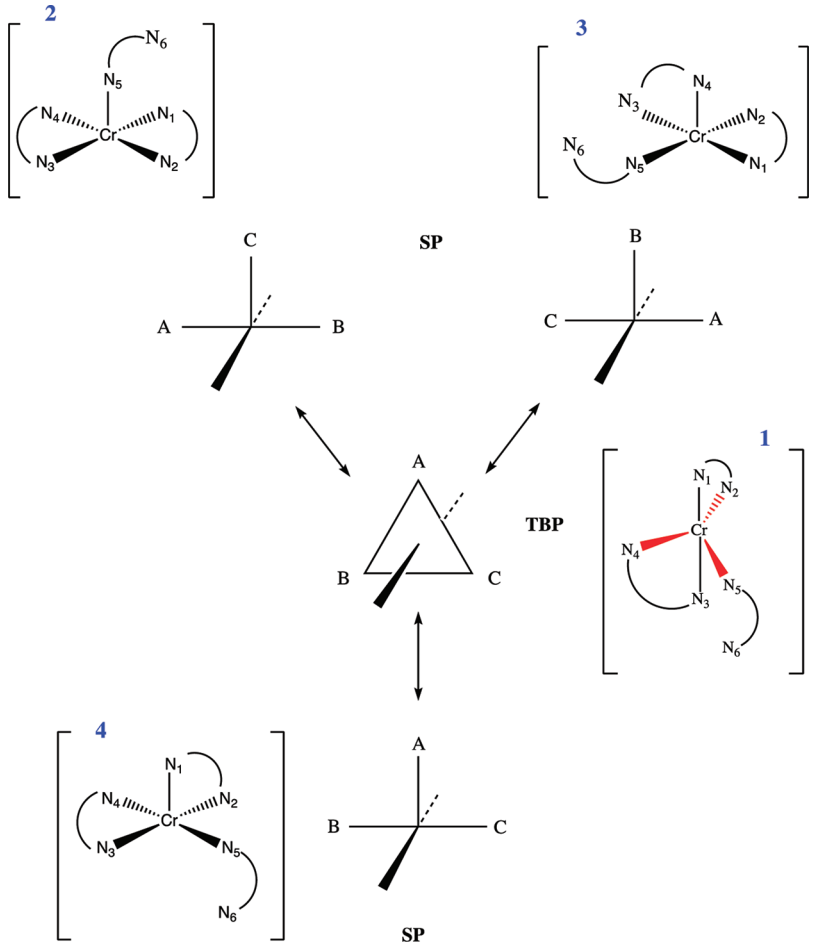

Figure 4. Isomerization pathways of trigonal bipyramidal (TBP) fragment to form square pyramidal (SPyr) structure. Red bonds represent the equatorial plane of the TBP system (adapted from ref 2).

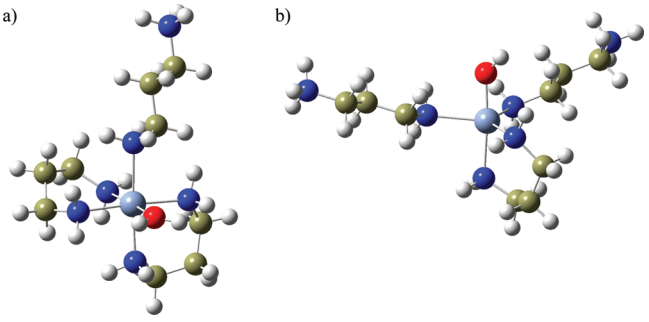

Figure 5. Structure of *cis*-$[Cr(tn)_2(tnH)(H_2O)]^{3+}$ at the point of (a) ground state minimum and (b) conical intersection.

via the JT-type vibrations (as described above) to form SPyr coordination at the metal center. After relaxing to the ground-state PES, the system can coordinate another water molecule to fill the coordination hole on the metal and thus form another photoproduct that was also experimentally detected, the $[Cr(tn)(tnH)_2(H_2O)_2]^{5+}$ complex. The same photoproduct could also be created through the quartet reaction pathway of the *trans* isomer of $[Cr(tn)_2(tnH)(H_2O)]^{3+}$.

The pathway for the formation of the diaquo species $[Cr(tn)_2(H_2O)_2]^{3+}$ was also examined. As was suggested earlier by Gowin and Wasgestian, the full dissociation of a tn ligand can occur via Jahn–Teller distortion in the excited electronic LF state.[13] The authors support this conclusion by the fact that one tetragonal plane in the $[Cr(tn)_3]^{3+}$ system (Figure 1c) contains one full tn ring and two nitrogen atoms that are linked to the axial position of the complex. Because the photoactive state should be equatorially labile, according to other studies for similar Cr amine systems, the bonds between Cr and N coming from the equatorial tn ring can break simultaneously. The vibrational modes of the $[Cr(tn)_3]^{3+}$ complex were studied using the B3LYP functional. The mode that favours full tn ligand dissociation was located and found to be a component of three close lying vibrations. This would support previous claims that the Jahn–Teller effect could be the reason for full tn dissociation. The ^4T photoactive excited state would couple through a Jahn–Teller active *t*-vibration (more precisely a component of a *t*-vibration coupled to $(a \oplus e)$electronic states for pseudo-D_3 systems). The vibrational modes that favor full dissociation of a tn ligand and dissociation of only one end are presented in the Table 3.

The $[Cr(tn)_3]^{3+}$ complex at the point of its conical intersection was taken, and the partially dissociated tn ligand was completely removed. A search of surface crossings on the quartet manifold of such a structure was then performed, and the same seam of conical intersection as for the full $[Cr(tn)_3]^{3+}$ complex was located (Figure 6).

The metal center at the point of conical intersection adopts a square planar geometry (SPlan). Figure 7 presents the orbitals splitting on moving from octahedral six-coordination to a square planar four-coordination geometry.

dx.doi.org/10.1021/jp302300q | J. Phys. Chem. A 2012, 116, 5375–5382

Table 3. Vibrational Modes for Full and Partial Dissociation of tn Ligand[a]

vibrational mode (cm^{-1})	assignment	vibrational symmetry
300.04	M−single N stretch	*e*
315.53	M−single N stretch	*e*
357.90	M−full tn stretch	*t*
371.62	M−full tn stretch	*t*
383.15	M−full tn stretch	*t*
402.34	M−full tn stretch (very small)	*a*
791.16	M−full tn stretch	*t*
795.58	M−full tn stretch	*t*
799.81	M−full tn stretch	*t*

[a]B3LYP functional used with SDD basis set for Cr and 6-31g(p,d) basis on the nonmetal atoms.

The population of electron density at the point of conical intersections for both $[Cr(tn)_3]^{3+}$ and $[Cr(tn)_2]^{2+}$ species is the same and presented in Table 2. The $d_{x^2-y^2}$ orbital is usually higher in energy for the SPlan geometry. The d_{xy} and d_{z^2} orbitals can be quasi-degenerate, and the electron can populate either of those. Thus, the conical intersection presented in Figure 6 is slightly distorted from a pure square planar structure to bring about the degeneracy of the states.

The $[Cr(tn)_2]^{2+}$ species was then optimized using the B3LYP functional on the ground-state potential energy surface (PES) after distortion along the gradient difference vector. The structure of the relaxed $[Cr(tn)_2]^{2+}$ species is presented in Figure 8. Water can then only coordinate to the metal center in the *cis* fashion forming *cis*-$[Cr(tn)_2(H_2O)_2]^{3+}$. Indeed only the *cis*-$[Cr(tn)_2(H_2O)_2]^{3+}$ photoproduct was observed experimentally.

Finally, the products of irradiation of the *cis*-$[Cr(tn)_2(H_2O)_2]^{3+}$ system were examined. After excitation to the quartet excited state, the system again reaches a Q_0/Q_1 conical intersection, with a quasi-TBP geometry. Here, dissociation of water is seen (Figure 9).

After relaxing to the ground-state PES, the system adopts again a SPyr geometry with a coordination hole at the metal center. The water molecule dissociated from the *cis* position could then, through the mechanism described before, recoordinate to a *cis* or *trans* position and form the initial system *cis*-$[Cr(tn)_2(H_2O)_2]^{3+}$ or the *trans*-$[Cr(tn)_2(H_2O)_2]^{3+}$

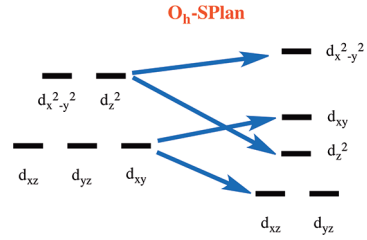

Figure 7. Splitting of metal 3d orbitals on moving from octahedral six-coordination to a square-planar four-coordination geometry.

isomer. We note that the *trans*-$[Cr(tn)_2(H_2O)_2]^{3+}$ isomer was not observed experimentally. So, this channel is clearly not favored in comparsion to the dissociative tn channels.

CONCLUSIONS

The photoaquation reaction of $[Cr(tn)_3]^{3+}$ and the formation of its photoproducts can be a multistep process. The first photoproducts formed are *cis* and *trans* monoaquo species $[Cr(tn)_2(tnH)(H_2O)]^{4+}$, and their irradiation leads to successive photolysis and formation of the other photoproducts including the diaquo species. The common feature of all monoaquo systems is the distortion of the quasi-octahedral coordination at the Cr(III) center to a quasi-trigonal bipyramid geometry, which is the lowest energy point of a surface crossing seam between the ground state and first quartet excited state. Due to Jahn−Teller-type distortions induced by this degeneracy, all these systems isomerize to form a square pyramidal geometry at the metal center with a coordination hole at the metal. After relaxation on the ground-state PES, the monoaquo species are formed by trapping of a water molecule at the coordination hole of the metal. Diaquo species can be formed by the Jahn−Teller induced conical intersection similar to a ($T \times t$) type involving a component of quartet T state and a component of a *t* vibration, which causes the dissociation of a full tn ligand, and after relaxation to the ground-state PES trapping of two water molecules at the metal center in the *cis* fashion only. Thus, our multiconfigurational results can help to explain the complex photochemistry observed in such systems. There is a similarity here with chromium oxalate that dissociates a single Cr−O bond to also form a five-coordinate intermediate that is a conical intersection between the ground- and excited-quartet species.[7] The difference there is that the

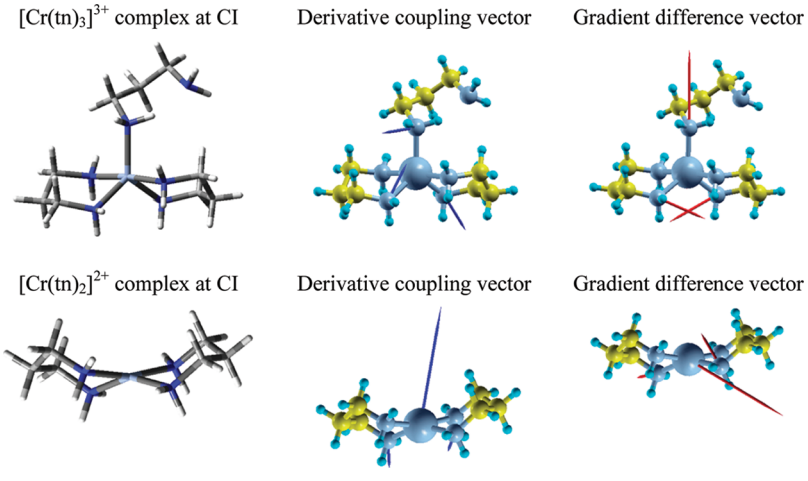

Figure 6. Conical intersection (Q_0/Q_1) structures with branching space vectors of $[Cr(tn)_3]^{3+}$ and $[Cr(tn)_2]^{2+}$ species.

dx.doi.org/10.1021/jp302300q | J. Phys. Chem. A 2012, 116, 5375−5382

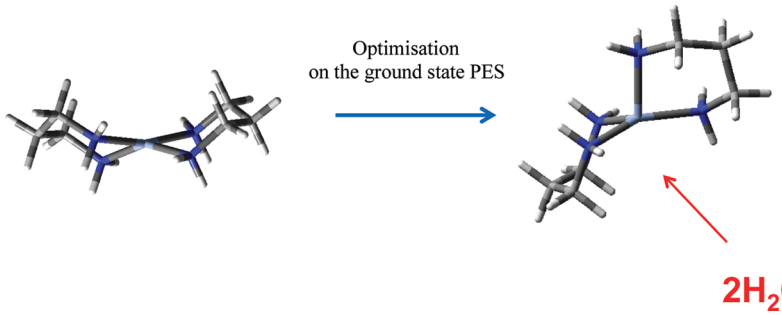

Figure 8. Ground-state optimized structure of the $[Cr(tn)_2]^{2+}$ species.

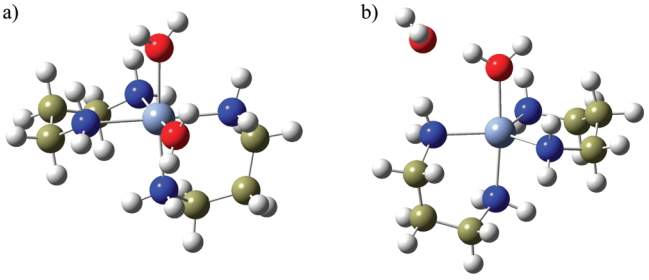

Figure 9. Structure of *cis*-$[Cr(tn)_2(H_2O)_2]^{3+}$ at the point of (a) ground state minimum and (b) conical intersection.

Cr−O bond can reform upon relaxation on the ground-state PES, whereas here, the long chain of the ligand has essentially unravelled taking the unbound amine too far away from the metal to reform the Cr−N bond and a water fills the coordination hole, thus giving photoaquation products. Such lower coordination conical intersections allowing for radiationless decay appear to be a common feature in Cr(III) photosystems.

■ ASSOCIATED CONTENT

Supporting Information

Structural parameters of $[Cr(tn)_3]^{3+}$ obtained in the calculations and from experimental studies. This material is available free of charge via the Internet at http://pubs.acs.org.

■ AUTHOR INFORMATION

Corresponding Author

*E-mail: m.j.paterson@hw.ac.uk.

Notes

The authors declare no competing financial interest.

■ ACKNOWLEDGMENTS

We thank the EPSRC for funding through grant EP/F01709X and the European Research Council (ERC) for funding under the European Union's Seventh Framework Programme (FP7/2007-2013)/ERC grant no. 258990.

■ REFERENCES

(1) Kirk, A. D.; Ibrahim, A. M. *Inorg. Chem.* **1990**, *29*, 4848.
(2) Vanquickenborne, L. G.; Coussens, B.; Postelmans, D.; Ceulemans, A.; Pierloot, K. *Inorg. Chem.* **1992**, *31*, 539.
(3) Kirk, A. D. *Chem. Rev.* **1999**, *99*, 1607.
(4) Kirk, A. D.; Irwin, G. *Coord. Chem. Rev.* **2001**, *211*, 25.
(5) Kane-Maguire, N. A. P. *Top. Curr. Chem.* **2007**, *280*, 37.
(6) Cimolino, M. C.; Linck, R. G. *Inorg. Chem.* **1981**, *20*, 3499.
(7) Żurek, J. M.; Paterson, M. J. *J. Chem. Phys.* **2011**, submitted for publication.
(8) Jurnak, F. A.; Raymond, K. N. *Inorg. Chem.* **1974**, *13*, 2387.
(9) Kirk, A. D.; Ibrahim, A. M. *Inorg. Chem.* **1988**, *27*, 4567.
(10) Kirk, A. D.; Frederick, L. A.; Glover, S. G. *J. Am. Chem. Soc.* **1980**, *102*, 7120.
(11) Kane-Maguire, N. A. P.; Wallace, K. C.; Miller, D. B. *Inorg. Chem.* **1985**, *24*, 597.
(12) Wong, C. F. C.; Kirk, A. D. *Can. J. Chem.* **1975**, *53*, 3388.
(13) Gowin, E.; Wasgestian, F. *Inorg. Chem.* **1985**, *24*, 3106.
(14) Kirk, A. D.; Fernando, S. R. L. *Inorg. Chem.* **1992**, *31*, 656.
(15) Kirk, A. D.; Fernando, S. R. L. *Inorg. Chem.* **1994**, *33*, 4435.
(16) Peterson, K. A. http://tyr0.chem.wsu.edu/~kipeters/basis.html.
(17) Bofill, J. M.; Pulay, P. *J. Chem. Phys.* **1989**, *90*, 3637.
(18) Pulay, P.; Hamilton, T. P. *J. Chem. Phys.* **1988**, *88*, 4926.
(19) Żurek, J. M.; Paterson, M. J. *J. Phys. Chem. Lett.* **2010**, *1*, 1301.
(20) Persson, B. J.; Roos, B. O.; Pierloot, K. *J. Chem. Phys.* **1994**, *101*, 6810.
(21) Paterson, M. J.; Hunt, P. A.; Robb, M. A.; Takahashi, O. *J. Phys. Chem. A* **2002**, *106*, 10494.
(22) Paterson, M. J.; Blancafort, L.; Wilsey, S.; Robb, M. A. *J. Phys. Chem. A* **2002**, *106*, 11431.
(23) Worth, G. A.; Welch, G.; Paterson, M. J. *Mol. Phys.* **2006**, *104*, 1095.
(24) McKinlay, R. G.; Paterson, M. J. The Jahn-Teller Effect in Binary Transition Metal Carbonyl Complexes. In *The Jahn-Teller Effect: Advances and Perspectives; Springer Series in Chemical Physics*; Köppel, H., Barentzen, H., Yarkony, D. R., Eds.; Springer: Heidelberg, Germany, 2010.
(25) McKinlay, R. G.; Żurek, J. M.; Paterson, M. J. *Adv. Inorg. Chem.* **2010**, *62*, 351.
(26) Żurek, J. M.; Paterson, M. J. *Inorg. Chem.* **2009**, *48*, 10652.
(27) Frisch, M. J. T., Trucks, G. W.; Schlegel, H. B.; Scuseria, G. E.; Robb, M. A.; Cheeseman, J. R.; Scalmani, G.; Barone, V.; Mennucci, B.; Petersson, G. A.; Nakatsuji, H.; Caricato, M.; Li, X.; Hratchian, H. P.; Izmaylov, A. F.; Bloino, J.; Zheng, G.; Sonnenberg, J. L.; Hada, M.; Ehara, M.; Toyota, K.; Fukuda, R.; Hasegawa, J.; Ishida, M.; Nakajima, T.; Honda, Y.; Kitao, O.; Nakai, H.; Vreven, T.; Montgomery, Jr., J. A.; Peralta, J. E.; Ogliaro, F.; Bearpark, M.; Heyd, J. J.; Brothers, E.; Kudin, K. N.; Staroverov, V. N.; Kobayashi, R.; Normand, J.; Raghavachari, K.; Rendell, A.; Burant, J. C.; Iyengar, S. S.; Tomasi, J.; Cossi, M.; Rega, N.; Millam, N. J.; Klene, M.; Knox, J. E.; Cross, J. B.; Bakken, V.; Adamo, C.; Jaramillo, J.; Gomperts, R.; Stratmann, R. E.; Yazyev, O.; Austin, A. J.; Cammi, R.; Pomelli, C.; Ochterski, J. W.; Martin, R. L.; Morokuma, K.; Zakrzewski, V. G.; Voth, G. A.; Salvador, P.; Dannenberg, J. J.; Dapprich, S.; Daniels, A. D.; Farkas, Ö.; Foresman, J. B.; Ortiz, J. V.; Cioslowski, J.; Fox, D. J. *Gaussian 09*, Revision A.1; Gaussian, Inc.: Wallingford, CT, 2009.